MOX-Report No. 21/2016

Mechanics and polarity in cell motility

Ambrosi, D.; Zanzottera, A.

MOX, Dipartimento di Matematica
Politecnico di Milano, Via Bonardi 9 - 20133 Milano (Italy)

mox-dmat@polimi.it http://mox.polimi.it

Mechanics and polarity in cell motility

D. Ambrosi, A. Zanzottera

MOX-Dipartimento di Matematica, Politecnico di Milano,
and Fondazione CEN, Piazza Leonardo da Vinci 32, 20133 Milano, Italy

Abstract

The motility of a fish keratocyte on a flat substrate exhibits two distinct regimes: the non-migrating and the migrating one. In both configurations the shape is fixed in time and, when the cell is moving, the velocity is constant in magnitude and direction. Transition from a stable configuration to the other one can be produced by a mechanical or chemotactic perturbation. In order to point out the mechanical nature of such a bistable behaviour, we focus on the actin dynamics inside the cell using a minimal mathematical model. While the protein diffusion, recruitment and segregation govern the polarization process, we show that the free actin mass balance, driven by diffusion, and the polymerized actin retrograde flow, regulated by the active stress, are sufficient ingredients to account for the motile bistability. The length and velocity of the cell are predicted on the basis of the parameters of the substrate and of the cell itself. The key physical ingredient of the theory is the exchange among actin phases at the edges of the cell, that plays a central role both in kinematics and in dynamics.

Introduction

The motility of eukariotic cells on flat substrates is conventionally described according to four phases: leading edge protrusion, adhesion to the substrate, contraction at the trailing edge and then retraction of the tail [6]. This scenario is however only stereotypical because for some cells, like fish keratocytes, these phases follow each other so rapidly that they are actually undistinguishable: all the steps occur simultaneously and the translation process is continuous in time. Moreover fish keratocytes exhibit two distinct motile regimes: in absence of external stimuli, they typically stay at rest with a rounded shape. A sufficiently large mechanical or chemotactical signal can trigger a destabilization that, in about 200 seconds, yields the cell to travel with constant velocity (up to 1 micron per second) and shape [7]. The same kinematics even characterizes the motion of a fragment of cell lamellipodium, with a lower speed ($\simeq 2-10$

micrometers per minute); as it lacks nucleus, microtubules and most organelles, the experiment suggests that the key elements of cell crawling are well represented even in such a simple system. The exhibited bistable behavior, signature of a nonlinear dynamics, is a fascinating challenge for the mathematical modelling of an active living mechanical system.

Both when the cell (or the lamellipodial fragment) is apparently at rest and when it is steadily migrating, the inner equilibrium of the mechanical system is actually dynamical: at a subcell level, the flow of free and polymerized actin follow patterns that have been unravelled during the last decades [3, 8]. Oligomeric actin (G–actin) freely diffuses in the cytosol and attaches to the barbed ends of the polymeric phase network (F–actin) that point outward the cell membrane; polymerized actin is backward transported by the myosin motors (retrograde flow). The vectorial sum of material velocity and growth velocity (polymerization rate) at the cell boundary produces the visible speed of the cell (which is possibly null). Free actin monomers detach from the actin network in the body of the cell and are passively transported by Brownian motion from regions of higher to regions of smaller concentration (namely the cell periphery, where the polymerization process acts as a sink for the G-actin) [9]. The free actin density correlates well with the high stress regions inside the cell, inhibition of the stress due to myosin activity slows down the cell, thus suggesting that the mechanical stress drives the depolymerization process [10, 23].

The shape of the boundary and the concentration patterns are very different between crawling and non crawling fragments. The fragment at rest is rounded, the lamellipodium has a symmetric shape, the actin cytoskeleton near the membrane grows at a constant rate and is backtransported from the boundary to the interior at the same velocity it is produced, so that the vectorial sum of velocities is zero. In a travelling fragment, the lamellipodium takes instead a characteristic canoe shape, the symmetry of actin and myosin concentration patterns is broken and the region of strong actomyosin activity is concentrated in the rear of the lamellipodium.

[Figure 1 about here.]

The polarization of the cell and the initiation of motility is strongly linked to the migration of several proteins on the plasma membrane and their spatial segregation. In particular, Rho GTPases are of crucial importance in regulating actin dynamics at the cell periphery [25]. Actin nucleation is typically the rate-limiting step in actin polymerization in vivo, so cells regulate where and when polymerization occurs by controlling the localization and activation of actin-nucleation promoting factors [27]. The polarity of the network is therefore instructed by the polarization of the membrane.

The mathematical modelling of cell migration has received an increasing attention over the last years. The evidence of a bistable behaviour is the signature of a nonlinearity that has been encoded in the models in terms of nonlinear constitutive equations for the cellular material. Alt and Dembo [1] and Kimpton et al [2] represent a cell as made of biphasic material, where the stress of the network has a spherical component which is cubic in the volume fraction. The nonlinearity of the constitutive equations determine the multiplicity of the stable regimes. According to Giomi and De Simone [19] a cell described as an active nematic droplet undergoes spontaneous division and motility thanks the phase separation favoured by the Ginzburg–Landau energy density and the nonlinearity of the Landau-deGennes free energy density. The theoretical aspects of cell motility can be addressed after homogenization of equations that detail the dynamics of the actin network, each filament being treated as an inextensible rod that resists to bending. Branching, capping, cross links and friction of the filaments of the network can be very naturally included in such a modelling framework [13]. Other approaches focus on the contraction-driven motility in a 1D cell: recent theoretical works based on the theory of active gels show that crawling is possible even without polymerization [11]. This particular mechanism of cell motility allows a precise formulation of the condition of optimal trade-off between performance and metabolic cost, so that the distribution of contractile elements can be recovered on the basis of an optimization argument [15]. The region at the leading edge, where the branched F-actin network is not stabilized by cross links, is very narrow when compared with the typical length of the lamellipodium: a few hundreds nanometers vs 10 micrometers [29]. An accurate mathematical modelling of such a flexible region is needed to get rid of the force-velocity relationship observed when a cell migrates on a flat substrate pushing a bending cantilever [30].

The mathematical model illustrated in this paper is inspired by Mori et al [28] and Larripa and Mogilner [14, 16], where the protein recruitment and segregation in the cytosol and on the membrane, the mechanics of the cytoskeleton and the treadmilling of actin are separately addressed. Here we formulate a minimal 1D theoretical model where the observed dynamics of free and polymerized actin in the cell is coupled with the stress actively produced by the myosin motors. The polarization of the cell follows the "wave pinning" model; the linear diffusion of proteins (namely Rho GTPases) on the plasma membrane and in cytosol and the nonlinear exchange between active (membrane-bound) and inactive (cytosolic) forms explains the existence of polar and non-polar stable states, while the (reversible) transitions among such states of the system occurs by finite perturbations [28]. The formation of a stationary front (the "wave pinning"), sharply separating the cell into two regions, mechanically identifies the polarity of the

F-actin network, where barbed ends do not point out of the cell in a radially symmetric way, but mostly in the direction of the motion. The novelty of our work is the focus on the mass conservation and momentum balance laws of the actin phases, supplemented by mass exchange and boundary flow, that all the components of the system must satisfy. While bistability is governed by diffusion and exchanges of proteins, we mechanically enforce the polarity of the cell in the boundary condition for the F-actin, relating its concentration to local amount of active proteins. The linearity of the constitutive equations allows to analytically compute stress and concentration fields, that are qualitatively in agreement with the observations. Our main result is the quantitative prediction of the length and the migration velocity of the cell fragment in the two stable configurations (cell at rest and motile cell) as a function of the physical parameters of the model.

1. The mathematical model

The lamellipodium of a fish keratocyte is a very thin structure, less than 1 micrometer thick vs. a width and a length of about 10-20 micrometers [31]. The shape of a cell at rest is almost cylindrical, while the shape of a steadily migrating cell exhibits a symmetry axis. Symmetry arguments and the corresponding high aspect ratios suggest to represent the cell as a one–dimensional strip, spanning the interval $(x_-(t), x_+(t))$ of the x axis, where the location of the boundaries is to be determined. In the following, all the relevant physical fields are therefore to be understood as averaged along the vertical and transverse direction.

The onset of polarity in a cell is due to membrane trafficking of a number of proteins. A minimal mathematical model able to capture the essential dynamics is provided by two reaction diffusion equations for a protein (Rho GTPases, for example) that diffuses with different rates on the membrane and in cytosol [28]

$$\begin{aligned} u_t - D_u u_{xx} &= f(u,w), \\ w_t - D_w w_{xx} &= -f(u,w), \end{aligned} \tag{1}$$

where $u(x,t)$ and $w(x,t)$ represent the concentration on the membrane and in the cytosol, respectively, $D_u \ll D_w$, and $f(u,w)$ is typically cubic in u. An elementary non–dimensional example is

$$f(u,w) = (u-u_0)(u-u_1)(u-u_2(w+1)), \tag{2}$$

where $u_2 > u_1 > u_0 > 0$ are constants. Both phases cannot outflow the cell

$$-D_u u_x\big|_{x_\pm} = -D_w w_x\big|_{x_\pm} = 0. \tag{3}$$

As the cytosolic phase w diffuses much faster than the one attached to the membrane, on the time scale of interest it has an homogeneous distribution, slaved to the dynamics of u by conservation arguments. The system has therefore two stable equilibrium states: a fully homogeneous one, where $u = u_0$, and a polarized one, when a steady front separates the two regions $u = u_0$ and $u = u_2(\bar{w} + 1)$, where $\bar{w}$ depends on the total protein amount and on the physical parameters. On the basis of this model, the onset of polarization is fully described in terms of active–inactive protein diffusion and exchange, and the state of polarization of a cell is "measured" by the value of u on its boundary.

Following [14], after vertical and transverse integration the actin cytoskeleton is here approximated as a one–dimensional viscous fluid with constant contractile active stress α,

$$\sigma = \mu v_x + \alpha, \tag{4}$$

where σ is the stress, μ the shear viscosity, $v(x,t)$ the vertically averaged horizontal velocity and the subscript denotes differentiation. While the actual rheology of the cytoskeleton is much more complex [21, 20], such a simple model is sufficient to point out some basic mechanisms of cell locomotion. Notice that both σ and α have the dimension of a force, while μ is a force multiplied by time. Moreover, in this simplified framework the myosin motors are supposed to be uniformly distributed in the cell body, so that α is a constant.

The interaction of the cell with the substrate is the shear stress between the cell membrane and the flat surface, here represented as a drag force proportional to the averaged velocity:

$$-\sigma_x = -\beta v, \tag{5}$$

where β is a frictional parameter. The dynamic boundary conditions in $x_\pm$ account for the tension of the cell membrane [27], assumed to be proportional to the cell length

$$\sigma_\pm = -\lambda L, \tag{6}$$

where $L(t) = x_+(t) - x_-(t)$ and we adopt the concise notation $\sigma_+ = \sigma(x_+)$ and so on. The parameter λ is a membrane elastic modulus (force per unit length) [4].

While the cell cytoskeleton is made of polymerized actin transported by the velocity v, the monomeric free actin diffuses in the cytosol; the monomers attach to the polymeric filaments at the cell leading edge, they detach in the body of the cell proportionally to the stress [23], so that the concentration of G–actin obeys the following reaction–diffusion equation

$$a_t - D a_{xx} = \kappa\sigma, \tag{7}$$

where D is the monomeric actin diffusivity in cytosol and κ is a constant. We assume that near the membrane the polymerization activity is regulated by the density of G-actin, which is proportional to the amount of proteins segregated on the membrane u:

$$a_{\pm} = \chi u_{\pm}, \tag{8}$$

where χ is a constant. According to the dynamics represented by equations (1) and (2), at equilibrium two scenarios show up: the boundary conditions are symmetric ($a_+ = a_-$) or they do not ($a_+ \neq a_-$), thus accounting for the polarity of the F-actin polymer [3]. We are therefore assuming that membrane trafficking of proteins regulates the polarization of the cell without mechanical feedback [26] and the polarity reflects in asymmetric boundary conditions for the G-actin.

The polymerized actin is backtransported by the material velocity v

$$a^p_t + \left(a^p v\right)_x = -\kappa\sigma. \tag{9}$$

As the cell is a closed system, the total actin is conserved; in other words the F-actin field is slaved to the G-actin one. Global conservation implies

$$\frac{d}{dt}\int_{x_-}^{x_+} (a + a^p)\, dx = \left[\dot{x}(a + a^p) + Da_x - va^p\right]_{x_-}^{x_+} = 0. \tag{10}$$

The concentration of polymerized actin can be therefore determined a posteriori solving equations (9) with boundary conditions (10) after that the free actin concentration $a(x,t)$ and the velocity field $v(x,t)$ have been determined.

Assuming that the concentration of the polymeric actin at the edge is fixed, say a_0, we get that the polymerization velocity at the boundary is proportional to the outflux of free actin,

$$\begin{aligned} -\dot{x}_+ a_+ - Da_x\big|_{x_+} &= v^p_+ a_0, \\ -\dot{x}_- a_- - Da_x\big|_{x_-} &= v^p_- a_0. \end{aligned} \tag{11}$$

The velocity of the cell boundaries $\dot{x}_{\pm}(t)$, the material velocity of the cell at the boundary $v_{\pm}(t)$ and the actin polymerization rate $v^p_{\pm}$ (the "growth velocity "of the cell) are related by

$$\dot{x}_{\pm} = v^p_{\pm} + v_{\pm}, \tag{12}$$

which are the kinematic boundary conditions.

[Figure 2 about here.]

The differential system is now closed: the elliptic-parabolic equations (5) and (7) are supplemented by the 2+2 boundary conditions (6) and (8), whereas the position of the boundaries of the cell are fixed by the kinematic conditions (12) supplemented by the constitutive assumption (11).

In the next sections we show that the above system of differential equations has one steady solution and two (symmetric) solutions of travelling wave type, where the length and the migration velocity of the cell satisfy algebraic equations that are explicitly stated.

2. Symmetric solution: cell at rest

A steady solution of the differential problem is defined in a constant spatial domain where all the physical fields are independent of time. The cell then spans the interval $(-L/2, L/2)$ of the x axis, fixed in time, where L is to be determined. The solution is expected to be symmetric with respect to the origin, so that considering the boundary conditions in one boundary point only (say $x = L/2$) is sufficient; as a matter of fact, L is the only boundary unknown as $\dot{x}_+ = 0$. Under these assumptions equation (5) can be readily integrated to give

$$v(x) = -\frac{\alpha + \lambda L}{\sqrt{\beta\mu}} \frac{\sinh\left(\sqrt{\frac{\beta}{\mu}}x\right)}{\cosh\left(\sqrt{\frac{\beta}{\mu}}\frac{L}{2}\right)}, \tag{13}$$

and

$$\sigma(x) = \alpha - (\alpha + \lambda L)\frac{\cosh\left(\sqrt{\frac{\beta}{\mu}}x\right)}{\cosh\left(\sqrt{\frac{\beta}{\mu}}\frac{L}{2}\right)}. \tag{14}$$

[Figure 3 about here.]

The plots of F-actin velocity and traction are shown in figures 3 and 4 for relevant sets of parameters, over corresponding lengths L (see below). The results compare well with the experimental data reported for an interval spanning 8 micrometers from the leading edge of the lamellipodium (see figure 2b in [18]).

The actin monomers density can be calculated by integrating equation (7), which reduces to

$$-Da_{xx} = \kappa\sigma. \tag{15}$$

As $\sigma(x)$ is an even function and $a_- = a_+$, it follows that $a(x)$ is even, too.

[Figure 4 about here.]

To determine the actin concentration at the boundary we integrate once equation (15)

$$-Da_x = \kappa g(x), \tag{16}$$

where $g(x) := \int_0^x \sigma$. Using the boundary condition (11) and the constitutive equation (16) we get

$$\kappa g_+ = a_0 v_+^p. \tag{17}$$

Using the known form of the stress (14), equation (17) explicitly rewrites as follows

$$a_0 v_+^p = \kappa \left(\alpha \frac{L}{2} - (\alpha + \lambda L)\sqrt{\frac{\mu}{\beta}} \tanh\left(\sqrt{\frac{\beta}{\mu}} \frac{L}{2} \right) \right). \tag{18}$$

The kinematic condition (12) then provides an algebraic equation for the length of the cell at rest

$$v_+ + \frac{\kappa}{a_0} g_+ = 0, \tag{19}$$

or explicitly,

$$\alpha \frac{L}{2} - (\lambda L + \alpha)\sqrt{\frac{\mu}{\beta}} \left(1 + \frac{a_0}{\kappa \mu} \right) \tanh\left(\sqrt{\frac{\beta}{\mu}} \frac{L}{2} \right) = 0. \tag{20}$$

The physical meaning of equation (19) is the following: given v and g as functions of the cell length, the boundary of the cell is fixed at $L/2$ such that the retrograde flow exactly balances the outflow of free actin (which rereads as elongation rate of the network polymerized actin). The same argument has been enforced by Etienne et al.: a competition of retrograde flow and protrusion, modulated by the stiffness of the environment, is the means by which cell area is regulated [24]. Because of the symmetry of the problem, the result (17) is notably independent of the boundary conditions (11) that are instead expected to play a role when the cell migrates.

There exists a unique, positive solution L of equation (20) if λ is sufficiently small, i.e. if the parameters satisfy the following inequality (see Appendix A)

$$\lambda < \frac{\alpha \kappa}{2} \frac{\sqrt{\beta \mu}}{(a_0 + \kappa \mu)}. \tag{21}$$

The existence condition (21) can be rewritten in a more perspicuous way

$$\left(1 + \frac{a_0}{\kappa \mu} \right) \lambda \sqrt{\frac{\mu}{\beta}} < \frac{\alpha}{2}. \tag{22}$$

The quantity $a_0/\kappa\mu$ represents the ratio between the material velocity v and the polymerization velocity v_p and it is known to be smaller than one. Therefore, neglecting the term in the bracket at the left hand side, condition (22) requires that the membrane tension, evaluated using the

representative viscous decay length $\sqrt{\mu/\beta}$ is much smaller than the active stress produced by the actomyosin machinery, a regime that definitely applies in a fish keratocyte.

A validation of the above theory comes from a comparison between the observed cell length and the one predicted according to (20), where physical measured parameters are employed. The values of the most relevant parameters used in the model are listed in Table 1, as extracted from the literature. On the basis of the smallness argument $a_0/\kappa\mu < 1$ illustrated above, the values of a_0 and κ have minor relevance.

[Table 1 about here.]

Figure 5 describes how the cell length changes when the model parameters are varied.

By using the parameters value extracted from the literature and reported in Table 1 we numerically compute $L \backsimeq 18\mu m$ which is consistent with the experimental results on fish keratocytes [32].

[Figure 5 about here.]

The G-actin density field can be obtained solving equation (15) with symmetric boundary conditions (8) (say $a_\pm = \chi u_1 = a_1$) thus giving

$$a(x) = \frac{\kappa}{D}\frac{\mu}{\beta}(\lambda L + \alpha)\left(\frac{\cosh\left(\sqrt{\frac{\beta}{\mu}}x\right)}{\cosh\left(\sqrt{\frac{\beta}{\mu}}\frac{L}{2}\right)} - 1\right) + \frac{\kappa}{D}\frac{\alpha}{2}\left(\frac{L^2}{4} - x^2\right) + a_1. \tag{23}$$

Figure 6 shows the free actin profile for a cell at rest. It is symmetric and the free actin concentrates at the center of the cell in correspondence to the maximum stress concentration, in agreement with observations.

[Figure 6 about here.]

3. Non-symmetric solution: polarized migrating cell

In this section we look for travelling wave type solutions of the system illustrated in Section 1. Our conjecture is that the polarity of the cell can be represented by an asymmetry in the boundary conditions for G-actin: the imbalance in actin polymerization at the boundaries drives the motion. To fix the ideas, we assume that the steady state solution of equation (8) is $a_+ = a_1, a_- = a_2$. All the fields are here supposed to depend on x and t in terms of the combination

$y = x - Vt$ where V is a constant to be determined; if a solution $V \neq 0$ exists, it corresponds to a motile cell. Then we assume

$$y_- = x_- - Vt = -L/2, \qquad y_+ = x_+ - Vt = L/2,$$

with L, V to be determined. The force balance equation involves no derivatives in time and the stress depends only on the spatial variations of the velocity, so that all the calculations of the previous sections and the results (13) and (14) for the velocity and stress field remain valid. We notice that $v(x)$ given by equation (13) is the velocity field of the cytoskeleton measured by an observer travelling with constant velocity V, while an observer at rest records $v(x) + V$.
The density of monomeric actin can now be calculated by solving equation (7), which here rewrites

$$-Va' - Da'' = \kappa\sigma. \tag{24}$$

In order to determine the actin concentration we integrate once equation (24)

$$-Va - Da' = \kappa g + c_1, \tag{25}$$

for which no symmetry argument in principle applies.
We look for solutions of equation (25) of the type

$$a(y) = h(y)\mathrm{e}^{-\frac{V}{D}y},$$

and we find

$$a(y) = c_2\mathrm{e}^{-\frac{V}{D}y} - \frac{c_1}{V} - \frac{\kappa}{D}\mathrm{e}^{-\frac{V}{D}y}\left(\int \mathrm{e}^{\frac{V}{D}y} g\right), \tag{26}$$

where c_1, c_2 are constants to be fixed enforcing the boundary conditions (8). In particular, we get

$$\begin{aligned} c_1 = -\frac{V}{2\sinh\left(\frac{V}{D}\frac{L}{2}\right)}\Bigg\{ & \frac{\kappa}{D}\left[\left(\int \mathrm{e}^{\frac{V}{D}y} g\right)_{L/2} - \left(\int \mathrm{e}^{\frac{V}{D}y} g\right)_{-L/2}\right] \\ & + a_1\mathrm{e}^{\frac{V}{D}\frac{L}{2}} - a_2\mathrm{e}^{-\frac{V}{D}\frac{L}{2}}\Bigg\} \end{aligned} \tag{27}$$

where V and L are to be determined on the basis of the kinematic boundary conditions.

[Figure 7 about here.]

[Figure 8 about here.]

The kinematic boundary conditions in a travelling frame of reference follow (11) and (12) when $\dot{x}_+ = V$

$$-Va_+ - Da_x\big|_{L/2} = (V - v_+)a_0, \tag{28a}$$

$$-Va_- - Da_x\big|_{-L/2} = (V - v_-)a_0. \tag{28b}$$

Since $v(y)$ is an odd function, subtracting the latter equations we find that the cell length is provided by

$$2v_+ + \frac{\kappa}{a_0}\int_{-L/2}^{L/2} \sigma \, dy = 0 \tag{29}$$

and we again recover the condition (19), which is independent of V.
In order to determine the velocity of the cell we sum equations (28a) and (28b) and get

$$(-Va - Da_x)_{L/2} + (-Va - Da_x)_{-L/2} = 2Va_0. \tag{30}$$

The physical meaning of equation (30) is transparent: motion can be produced only by an imbalance of actin flow at the border. We recall the form of the fluxes (11): by using the integral (25) and the fact that g is an odd function we get

$$a_0 V = c_1. \tag{31}$$

or, using equation (27)

$$a_0 V = \frac{-V}{2\sinh\left(\frac{V}{D}\frac{L}{2}\right)}\left\{\frac{\kappa}{D}\left[\left(\int \mathrm{e}^{\frac{V}{D}y} g\right)_{L/2} - \left(\int \mathrm{e}^{\frac{V}{D}y} g\right)_{-L/2}\right] + a_1 \mathrm{e}^{\frac{V}{D}\frac{L}{2}} - a_2 \mathrm{e}^{-\frac{V}{D}\frac{L}{2}}\right\} \tag{32}$$

After discarding the $V = 0$ solution, corresponding to the case $c_1 = 0$ explored in the previous section, we finally determine the condition that fixes the velocity of the travelling cell

$$2a_0 \sinh\left(\frac{V}{D}\frac{L}{2}\right) = \frac{-\kappa}{D}\left[\left(\int \mathrm{e}^{\frac{V}{D}y} g\right)_{L/2} - \left(\int \mathrm{e}^{\frac{V}{D}y} g\right)_{-L/2}\right] - \left(a_1 \mathrm{e}^{\frac{V}{D}\frac{L}{2}} - a_2 \mathrm{e}^{-\frac{V}{D}\frac{L}{2}}\right) \tag{33}$$

where L is the unique solution of equation (29). In Appendix B it is shown that for $a_2 > a_1$ the algebraic equation (33) has a unique positive solution V; viceversa $-V$ is solution when a_1 and a_2 are exchanged.

[Figure 9 about here.]

In Figure 9 the migration velocity predicted by equations (29) and (33) is plotted versus some relevant parametric combinations. The migration velocity ranges the interval 0.1-0.3 micrometers per second, consistently with the observations [30, 32, 33]. As could be expected, V diminishes

linearly with λ and grows linearly with the G-actin diffusion coefficient D, but it is damped more than linearly versus the viscous diffusion length $\sqrt{\mu/\beta}$. The dependence of V versus the active stress and versus the ratio between material velocity and growth velocity provide remarkable information, that could not be foreseen without the support of a mathematical model. In fact, V grows versus α according to a curve that saturates at $V \simeq .3\ \mu m\ s^{-1}$ around the value of 400 pN, thus suggesting that the migration velocity weakly depends on the active stress. Conversely, the very rapid growth of V when $a_0/\kappa\mu \to 0$, prompts the conjecture that the retrograde velocity plays a stabilizing role in cell mechanics, keeping the value of V in the portion of the curve at the right of the parametric value $a_0/\kappa\mu \simeq 0.2$.

According to equation (29), a migrating fish keratocyte has the same size of a cell at rest; while this is physically nearly true, we observe that such an approximation is due to the simplicity of our model, that does not account for the stress field generated by an asymmetric pattern of myosin. Our approach is therefore complementary to Recho et al [12], who focus on the initiation of motility as driven by contraction only. While the introduction of a dependence of the stress field on the myosin concentration in equation (4) would be straightforward, the solution of the equations should be written in terms of special functions, and the final results would not be that transparent. More important, equation (33) suggests that the key ingredient to sustain the cell motility is the imbalance of actin flow between leading and trailing edge. The (symmetric) stress field however plays a fundamental role in determining the actin depolymerization rate, which is maximum far from the lamellipodium edge. While actin, myosin and adhesion orchestrate the transition from (apparently) static to migrating cell [17], the nonlinearity of the actin flux at the boundaries, that reflects the polarity of the polymeric chain, is sufficient to feed the locomotion machinery of the polarized cell.

As observed in Section 1, the profile of F-actin $a^p(y)$ can now be calculated a posteriori. In a travelling frame of reference equation (9) rewrites

$$((v - V)a^p)_y = -\kappa\sigma. \tag{34}$$

As we are interested in the physical regime $|V| > |v|$, the quantity $v - V$ always has the sign of $-V$ on the boundary. Assuming, for instance, that $V > 0$, the characteristics enter the right boundary and therefore equation (34) has to be integrated between in $[y, L/2]$,

$$(v - V)a^p = [(v - V)a^p]_{L/2} + \kappa \int_y^{L/2} \sigma \tag{35}$$

or,

$$a^p(y) = \frac{-\left[-Va - Da'\right]_{L/2} + \kappa \int_y^{L/2} \sigma}{v - V}, \tag{36}$$

where the boundary condition (28a) has been used. The profile of G-actin according to equation (36) is plotted in figure 10.

[Figure 10 about here.]

A comparison of the plots n figures 7 and 10 with experimental curves [34] reveals qualitative analogies: the concentration of F-actin as a function of the distance from the leading edge exhibits a peak and then a rapid decay, while the slope of the G-acin curve is mild and almost constant.

Final remarks

A fragment of lamellipodium of fish keratocyte is a very attractive minimal biophysical system to investigate the physics of cell motility. We have formulated a mathematical model that accounts for the basic mechanisms that drive the crawling of a lamellipodial fragment. While polarization of the cell is governed by a bistable reaction–diffusion equation accounting for the trafficking of proteins on the plasma membrane and in the cytosol, the concentration of active proteins dictates the polymerization rate at the edges of the cell. Our contribution is in coupling this reaction–diffusion system with mechanics: the stress modulates the F-actin depolymerization rate in bulk while the exchange between actin phases near the membrane is governed by the concentration of active proteins. In particular, in a polarized cell, the imbalance in the exchange between F-actin and G-actin produces the displacement.

The mathematical model illustrated in this work has a number of physical and biological limitations. Traction force microscopy reveals that when a fish keratocyte travels, the largest stress occurs in the transverse direction [10]; this compressive pattern, which is probably instrumental to the stabilization of the trajectory and to the rearward depolymerization of the cytoskeletal network, is ruled out by our transverse average. Moreover the active stress is here supposed to be independent of the position, while information about the non-homogeneous distribution of myosin motors are known. Last, but not least, the polarization dynamics and the stress pattern are here fully decoupled: the diffusion of proteins on the membrane drives the polarity of the cell generating an asymmetric concentrations of G-actin at the boundary without any feedback. This is the current paradigm in molecular biology [25, 26]. However it could be interesting to investigate the role of myosin contractility during the transient polarization process: when the

cell passes from the state at rest to the motile one the actin network reorganizes and forces play a role which might be not purely slaved to the dynamics of proteins on the membrane. Such a regime is immaterial for the present work where only steady states are considered.

Another mechanical issue not addressed in the present work is the force produced by a cell against an obstacle to move, a framework of paramount relevance in the perspective of 3D migration. In the particular case of a stalled cell, the retrograde velocity is approximately equal to the polymerization velocity of a free cell [30]. This demonstrates that in more complex scenarios, when external loads are applied, the mechanics produces a feedback on the polymerization rate that is not captured by the present model.

Notwithstanding only few physical ingredients have been introduced, a number of analytical results have been obtained. The linear equations representing the balance of mass of free actin and the balance of momentum for the polymerized actin, can be integrated, thus providing profiles of concentration, velocity and stress that compare well with the observed ones. All the nonlinearity of the system, needed to account for the observed bistability, is encoded in the bistable reaction–diffusion system that governs the phase exchanges (oligomeric vs. polymeric) at the boundary, i.e. in the kinematic and dynamic boundary conditions. The use of linear constitutive equations allows to find a closed (algebraic) form for the dependence of the length and speed of a fragment on the parameters of the model which account for the observed bistability. Using values of the physical parameters taken from the literature, we find that our predictions agree with the reported ranges, thus backward supporting the validity of the overall theoretical model.

Acknowledgments

We are indebted with Paolo Biscari and Pasquale Ciarletta for fruitful discussions about the content of this paper. This work was partially supported by the Start-up Packages and PhD Program project, co-funded by Regione Lombardia through the Fondo per lo sviluppo e la coesione 20072013 -formerly FAS.

Appendix

Appendix A

Let

$$f(L) := -\tanh\left(\sqrt{\frac{\beta}{\mu}}\frac{L}{2}\right)(\lambda L+\alpha)\left(\frac{1}{\sqrt{\beta\mu}}+\frac{\kappa}{a_0}\sqrt{\frac{\mu}{\beta}}\right)+\frac{\kappa\alpha}{a_0}\frac{L}{2}$$

the left hand side of (20). Notice that

$$f(0) = 0\,, \qquad f'(0) = -\frac{\alpha}{2\mu} < 0,\ \forall\ \alpha, \mu > 0.$$

Moreover,

$$\lim_{L\to+\infty} f(L) = \lim_{L\to+\infty} L\left(-\lambda\left(\frac{1}{\sqrt{\beta\mu}} + \frac{\kappa}{a_0}\sqrt{\frac{\mu}{\beta}}\right) + \frac{\kappa\alpha}{2a_0}\right).$$

Therefore if $\lambda < \dfrac{\alpha\kappa}{2}\dfrac{\sqrt{\beta\mu}}{(a_0+\kappa\mu)}$, there exists a positive solution L of (20).

Appendix B

Let

$$\begin{aligned} f(V) :=& -2Va_0 - V\frac{\left(a_1 e^{\frac{V}{D}\frac{L}{2}} - a_2 e^{-\frac{V}{D}\frac{L}{2}}\right)}{\sinh\left(\frac{V}{D}\frac{L}{2}\right)} - \frac{\kappa\alpha L}{\tanh\left(\frac{V}{D}\frac{L}{2}\right)} + \\ &+ 2V^2\kappa\mu\sqrt{\frac{\mu}{\beta}}\frac{(\lambda L+\alpha)}{(V^2\mu-\beta D^2)}\frac{\tanh\left(\sqrt{\frac{\beta}{\mu}}\frac{L}{2}\right)}{\tanh\left(\frac{V}{D}\frac{L}{2}\right)} - \frac{2\kappa D(D^2\alpha\beta + V^2\mu\lambda L)}{V(V^2\mu-\beta D^2)} \end{aligned}$$

the explicit expression of left hand side of (33). Notice that

$$\lim_{V\to 0^+} f(V) = \frac{-2D(a_1-a_2)}{L}\,, \quad \lim_{V\to+\infty} f(V) = -\infty.$$

Therefore if $a_1 < a_2$ there exists a positive solution V of (33).

[1] Alt W and Dembo M, Cytoplasm dynamics and cell motion: two-phase flow models, Mathematical Biosciences, 156:207228 (1999).

[2] Kimpton LS, Whiteley JP, Waters SL, King JR and Oliver JM, Multiple travelling-wave solutions in a minimal model for cell motility, Mathematical Medicine and Biology, 30:241-272 (2013).

[3] Mogilner A, Mathematics of cell motility: have we got its number?, J. Math. Biol., 58:105134 (2009).

[4] Diz-Muñoz A, Fletcher DA, and Weiner OD, Use the force: membrane tension as an organizer of cell shape and motility. Trends in cell biology, 23, 2, 47–53 (2013).

[5] Kruse K, Joanny JF, Julicher F and Prost J, Contractility and retrograde flow in lamellipodium motion. Physical Biology, 3, 130–137, (2006).

[6] Alberts B, Johnson A, Lewis J. et al. Molecular Biology of the Cell, 4e. Garland Science (2002).

[7] Verkhovsky AB, Svitkina TM and Borisy GG, Self-polarization and directional motility of cytoplasm, Curr Biol 9(1):11-20 (1999)

[8] Rubinstein B, Fournier MF, Jacobson K, Verkhovsky AB and Mogilner A, Actin-myosin viscoelastic flow in the keratocyte lamellipod, Biophysical J, 97(7):1853-1863 (2009).

[9] Mogilner A and Oster G, Cell motility driven by actin polymerization, Biophys J, 71:3030-3045 (1996).

[10] Fournier MF, Sauser R, Ambrosi D, Meister JJ and Verkhovsky AB, Force transmission in migrating cells, J Cell Biology, 188(2):287-297 (2010).

[11] Recho P, Putelat T and Truskinovsky L, Contraction-Driven Cell Motility, Phys Rev Lett, 111:108102 (2013)

[12] Recho P, Putelat T and Truskinovsky L, Motility initiation in active gels, arXiv:1501.07185v1

[13] Oelz D and Schmeiser C, Simulation of lamellipodial fragments, J Math Biol, 64:513-528 (2012)

[14] Larripa K and Mogilner A, Transport of a 1D viscoelastic actinmyosin strip of gel as a model of a crawling cell, Physica A, 372(1):113-123 (2006).

[15] Recho P, Joanny JF and Truskinovsky L, Optimality of contraction-driven crawling, Phys Rev Lett, 112:218101 (2014)

[16] Novak IL, Slepchenko BM and Mogilner A, Quantitative Analysis of G-Actin Transport in Motile Cells, Biophysical Journal. 95(4):1627-1638 (2008).

[17] Barnhart E, Lee KC, Allen GM, Theriot JA and Mogilner A, Balance between cellsubstrate adhesion and myosin contraction determines the frequency of motility initiation in fish keratocytes PNAS 112:5045-5050 (2015).

[18] Craig EM, Stricker J, Gardel M and Mogilner A, Model for adhesion clutch explains biphasic relationships between actin flow and traction at the cell leading edge, Phys Biol, 12:035002 (2015).

[19] Giomi L and DeSimone A, Spontaneous division and motility in active nematic droplets, PRL 112:147802 (2014).

[20] Ambrosi D and Ciarletta P, Plasticity in passive cell mechanics, Int J Non-Linear Mech, 56:56-60 (2013).

[21] Pullarkat PA, Fernandez PA and Ott A, Rheological properties of the Eukaryotic cell cytoskeleton, Physics Reports 449:2953 (2007).

[22] Adler Y and Givli S, Closing the loop: Lamellipodia dynamics from the perspective of front propagation, Physical Review E 88.4 (2013): 042708.

[23] Wilson CA, Tsuchida MA, Allen GM, Barnhart EL, Applegate KT, Yam PT, Lin Ji, Keren K, Danuser G and Theriot JA, Myosin II contributes to cell–scale actin network treadmilling through network disassembly, Nature 465:373–377 (2010).

[24] Étienne J, Fouchard J, Mitrossilis D, Bufi N, Durand-Smet P and Asnacios A, Cells as liquid motors: Mechanosensitivity emerges from collective dynamics of actomyosin cortex, PNAS, 112(9):2740-2745 (2015).

[25] Ridley AJ, Rho GTPases and actin dynamics in membrane protrusions and vesicle trafficking, Trends Cell Biol, 16:522529 (2006).

[26] Ridley AJ, Life at the leading edge, Cell, 145(7):1012-1022 (2011).

[27] Keren K, Cell motility: the integrating role of the plasma membrane, Eur Biophys J, 40(9):1013-1027 (2011).

[28] Mori Y, Jilkine A and Edelstein-Keshet L, Wave pinning and cell polarity from a bistable reaction–diffusion system, Biophys J, 94:3684–3697 (2008).

[29] Zimmermann J, Enculescu M and Falcke M, Leading–edge–gel coupling in lamellipodium motion, Physical Review E, 82(5):051925 (2010).

[30] Zimmermann J, Brunner C, Enculescu M, Goegler M, Ehrlicher A, Käs J and Falcke M, Actin filament elasticity and retrograde flow shape the force-velocity relation of motile cells. Biophysical J, 102(2):287-295 (2012).

[31] Small JV, Stradal T, Vignal E and Rottner K, The lamellipodium: where motility begins, Trends in cell biology, 12(3):112-120 (2002).

[32] Vallotton P, Danuser G, Bohnet S, Meister JJ and Verkhovsky AB, Tracking retrograde flow in keratocytes: news from the front, Molecular biology of the cell, 16(3):1223-1231 (2005).

[33] Jurado C, Haserick JR and Lee J, Slipping or gripping? Fluorescent speckle microscopy in fish keratocytes reveals two different mechanisms for generating a retrograde flow of actin. Molecular biology of the cell, 16(2):507-518 (2005).

[34] Koestler SA, Rottner K, Lai F, Block J, Vinzenz M and Small JV, F-and G-actin concentrations in lamellipodia of moving cells. PloS one, 4(3):e4810 (2009).

List of Figures

1 Velocity pattern in a fish keratocyte at rest (left) and in a migrating one (right) (sketch from figure 1 in [23]). In the cell at rest, the material velocity v (in red) balances the growth velocity v_p (in green) at the boundary; in a migrating cell the sum of the contributions imbalance at the boundary and gives rise to the steady motion with velocity V which is the vectorial sum of the two contributions [22]. . 20

2 Velocity pattern in a minimal one–dimensional model of a cell (blue) on a flat substrate (light blue). The generic non–equilibrium configuration corresponds to a cell length $L(t) = x_+(t) - x_-(t)$ moving with speed $V(t) = (\dot{x}_+(t) + \dot{x}_-(t))/2$ (left). The two possible equilibrium configurations are the cell at rest (center) and the cell migrating with constant speed V and length (right). The material and polymerization velocities are plotted in green and red, respectively. The cell at rest is characterized by symmetric velocity fields (center), while motility emerges from the symmetry breaking (left and right). 21

3 Cell at rest: spatial distributions of F-actin velocity for relevant sets of parameters. Green line: $\alpha = 0.8 \cdot 10^3$, $\beta = 0.9 \cdot 10^4$, $\mu = 5.5 \cdot 10^5$, $\lambda = 0.5$, $\frac{a_0}{\kappa\mu} = 0.33$. Red line: $\alpha = 0.6 \cdot 10^3$, $\beta = 1.1 \cdot 10^4$, $\mu = 5.5 \cdot 10^5$, $\lambda = 0.9$, $\frac{a_0}{\kappa\mu} = 0.45$. Magenta line: $\alpha = 0.4 \cdot 10^3$, $\beta = 1.1 \cdot 10^4$, $\mu = 5.5 \cdot 10^5$, $\lambda = 0.9$, $\frac{a_0}{\kappa\mu} = 0.4$. 22

4 Cell at rest: spatial distribution of traction for relevant sets of parameters. Green line: $\alpha = 0.8 \cdot 10^3$, $\beta = 0.9 \cdot 10^4$, $\mu = 5.5 \cdot 10^5$, $\lambda = 0.5$, $\frac{a_0}{\kappa\mu} = 0.33$. Red line: $\alpha = 0.6 \cdot 10^3$, $\beta = 1.1 \cdot 10^4$, $\mu = 5.5 \cdot 10^5$, $\lambda = 0.9$, $\frac{a_0}{\kappa\mu} = 0.45$. Magenta line: $\alpha = 0.4 \cdot 10^3$, $\beta = 1.1 \cdot 10^4$, $\mu = 5.5 \cdot 10^5$, $\lambda = 0.9$, $\frac{a_0}{\kappa\mu} = 0.4$. 23

5 Plots of the cell length as a function of the relevant parametric combinations (a) $\frac{\lambda}{\alpha}$, (b) $\sqrt{\frac{\mu}{\beta}}$, (c) $\frac{a_0}{\kappa\mu}$. The fixed parameters take the values given in table 1. In Figure 5 (a) and Figure 5(b) $\frac{a_0}{\kappa\mu} = 0.33$. 24

6 Cell at rest: spatial distribution of monomeric actin for values of model parameters listed in table 1. Here $a_0/a_1 = 3.6$; $a_0/\kappa\mu = 0.36$. 25

7 Migrating cell: spatial distribution of monomeric actin for a cell moving in the positive x direction with different (given) migration velocities. Actin distributions are normalized using the value at the leading edge: $a(L/2) = a_1 = 5 \cdot 10^6$, $a(-L/2) = a_2$. We set $a_2 = 1.0078\, a_1$ (black line), $a_2 = 1.82\, a_1$ (red line), $a_2 = 3.75\, a_1$ (blue line), $a_2 = 8.1\, a_1$ (green line), $a_2 = 18.3\, a_1$ (magenta line). Moreover $a_0/\kappa\mu = 0.36$. The remaining model parameters take the values listed in table 1. 26

8 Migrating cell: spatial distribution of monomeric actin for a cell moving in the positive x direction with different migration velocities. Actin distributions are normalized by their maximal absolute values. In each computation $a(L/2) = a_1$, $a(-L/2) = a_2$ with $a_1 = 5 \cdot 10^6$. We set $a_2 = 1.0078\, a_1$ (black line), $a_2 = 1.82\, a_1$ (red line), $a_2 = 3.75\, a_1$ (blue line), $a_2 = 8.1\, a_1$ (green line), $a_2 = 18.3\, a_1$ (magenta line). Moreover $a_0/\kappa\mu = 0.36$. The remaining model parameters take the values listed in table 1. 27

9 Cell velocity as a function of: (a) α, (b) $\frac{a_0}{\kappa\,\mu}$, (c) λ, (d) D, (e) $\sqrt{\frac{\mu}{\beta}}$. In each computation the fixed parameters take the values given in table 1. Moreover, we set $a(\frac{L}{2}) = a_1 = 5 \cdot 10^6$, $a(-\frac{L}{2}) = a_2 = 4a_1$ and in (a), (b), (c), (d) $\frac{a_0}{\kappa\mu} = 0.33$. . . 28

10 Migrating cell: spatial distribution of polymeric actin for a cell moving in the positive x direction according to (36). Actin distributions is normalized by its maximal value. All the parameters are as listed in table 1. 29

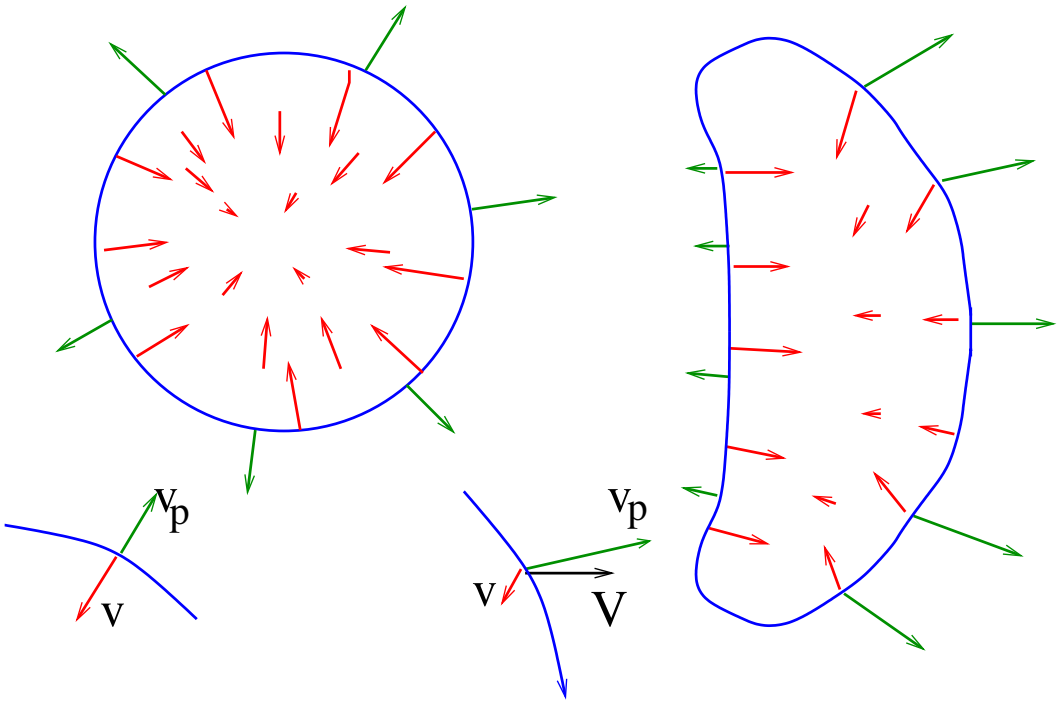

Figure 1: Velocity pattern in a fish keratocyte at rest (left) and in a migrating one (right) (sketch from figure 1 in [23]). In the cell at rest, the material velocity v (in red) balances the growth velocity v_p (in green) at the boundary; in a migrating cell the sum of the contributions imbalance at the boundary and gives rise to the steady motion with velocity V which is the vectorial sum of the two contributions [22].

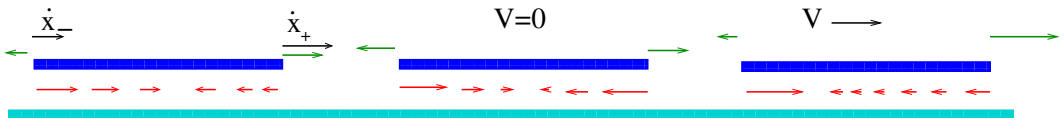

Figure 2: Velocity pattern in a minimal one–dimensional model of a cell (blue) on a flat substrate (light blue). The generic non–equilibrium configuration corresponds to a cell length $L(t) = x_+(t) - x_-(t)$ moving with speed $V(t) = (\dot{x}_+(t) + \dot{x}_-(t))/2$ (left). The two possible equilibrium configurations are the cell at rest (center) and the cell migrating with constant speed V and length (right). The material and polymerization velocities are plotted in green and red, respectively. The cell at rest is characterized by symmetric velocity fields (center), while motility emerges from the symmetry breaking (left and right).

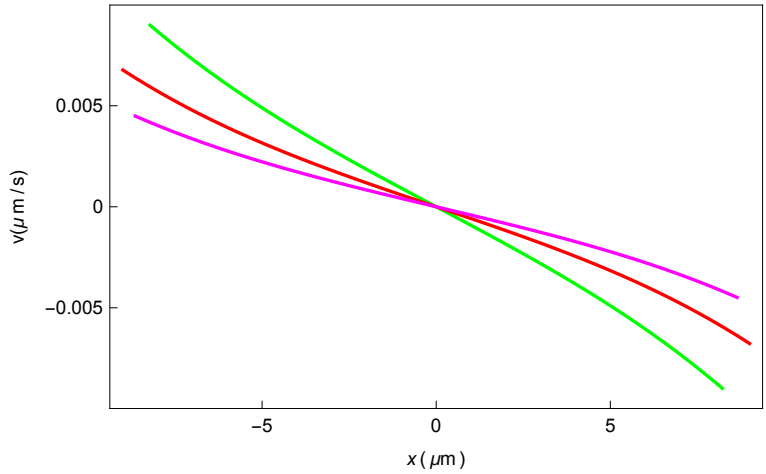

Figure 3: Cell at rest: spatial distributions of F-actin velocity for relevant sets of parameters. Green line: $\alpha = 0.8 \cdot 10^3$, $\beta = 0.9 \cdot 10^4$, $\mu = 5.5 \cdot 10^5$, $\lambda = 0.5$, $\frac{a_0}{\kappa\mu} = 0.33$. Red line: $\alpha = 0.6 \cdot 10^3$, $\beta = 1.1 \cdot 10^4$, $\mu = 5.5 \cdot 10^5$, $\lambda = 0.9$, $\frac{a_0}{\kappa\mu} = 0.45$. Magenta line: $\alpha = 0.4 \cdot 10^3$, $\beta = 1.1 \cdot 10^4$, $\mu = 5.5 \cdot 10^5$, $\lambda = 0.9$, $\frac{a_0}{\kappa\mu} = 0.4$.

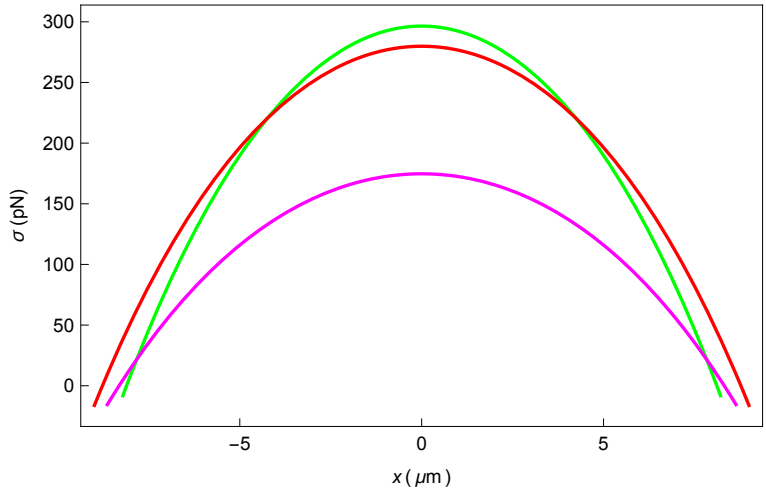

Figure 4: Cell at rest: spatial distribution of traction for relevant sets of parameters. Green line: $\alpha = 0.8 \cdot 10^3$, $\beta = 0.9 \cdot 10^4$, $\mu = 5.5 \cdot 10^5$, $\lambda = 0.5$, $\frac{a_0}{\kappa\mu} = 0.33$. Red line: $\alpha = 0.6 \cdot 10^3$, $\beta = 1.1 \cdot 10^4$, $\mu = 5.5 \cdot 10^5$, $\lambda = 0.9$, $\frac{a_0}{\kappa\mu} = 0.45$. Magenta line: $\alpha = 0.4 \cdot 10^3$, $\beta = 1.1 \cdot 10^4$, $\mu = 5.5 \cdot 10^5$, $\lambda = 0.9$, $\frac{a_0}{\kappa\mu} = 0.4$.

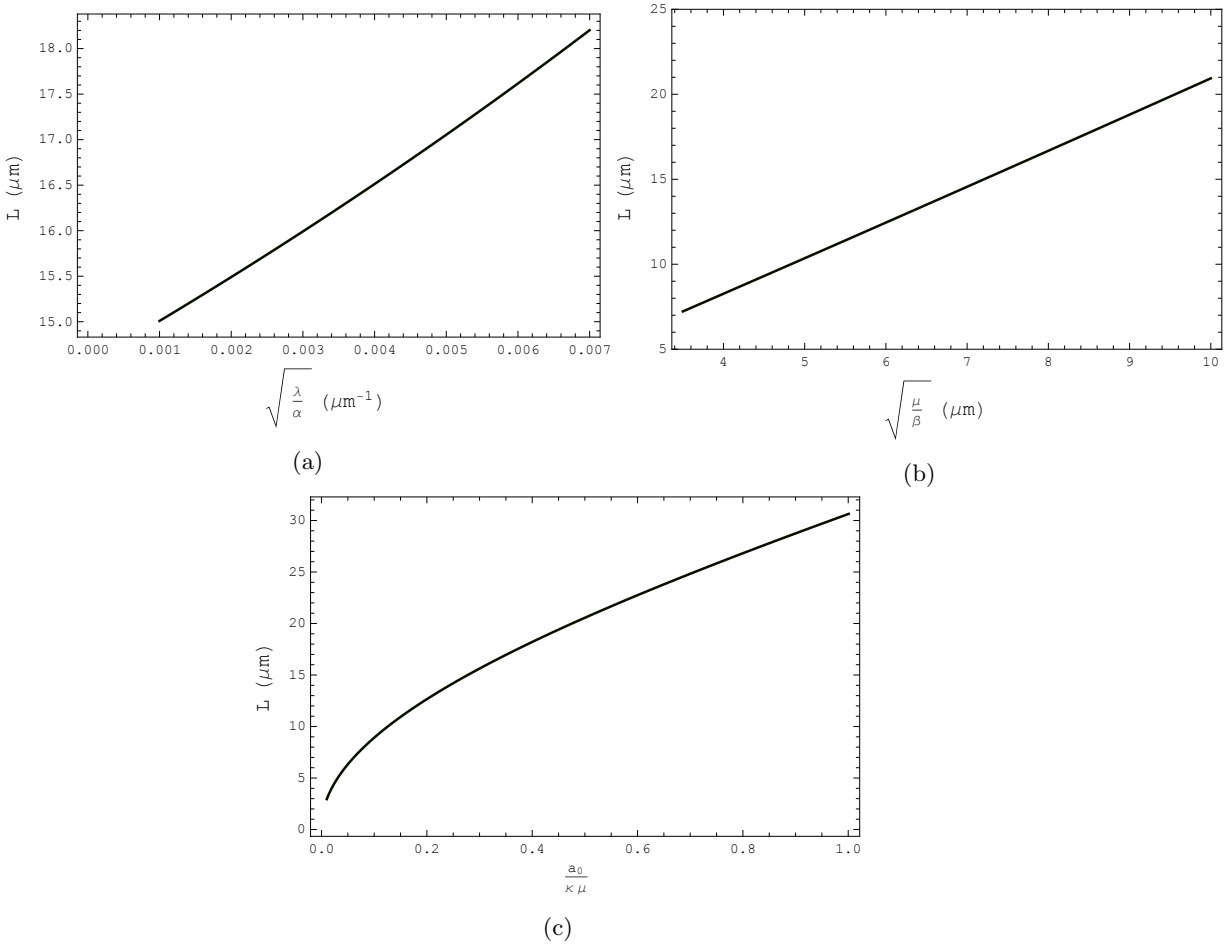

Figure 5: Plots of the cell length as a function of the relevant parametric combinations (a) $\frac{\lambda}{\alpha}$, (b) $\sqrt{\frac{\mu}{\beta}}$, (c) $\frac{a_0}{\kappa\mu}$. The fixed parameters take the values given in table 1. In Figure 5 (a) and Figure 5(b) $\frac{a_0}{\kappa\mu} = 0.33$.

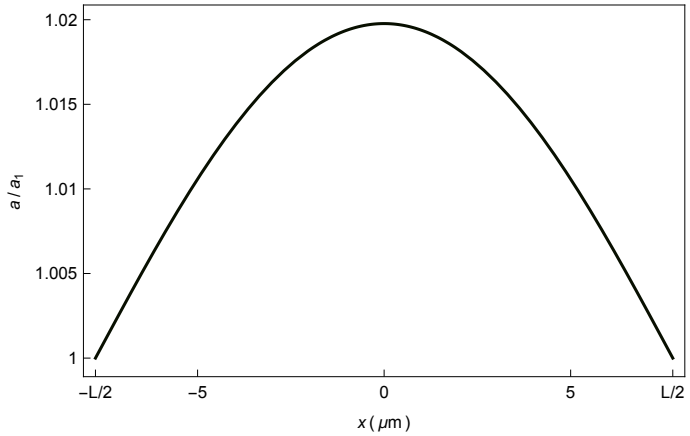

Figure 6: Cell at rest: spatial distribution of monomeric actin for values of model parameters listed in table 1. Here $a_0/a_1 = 3.6$; $a_0/\kappa\mu = 0.36$.

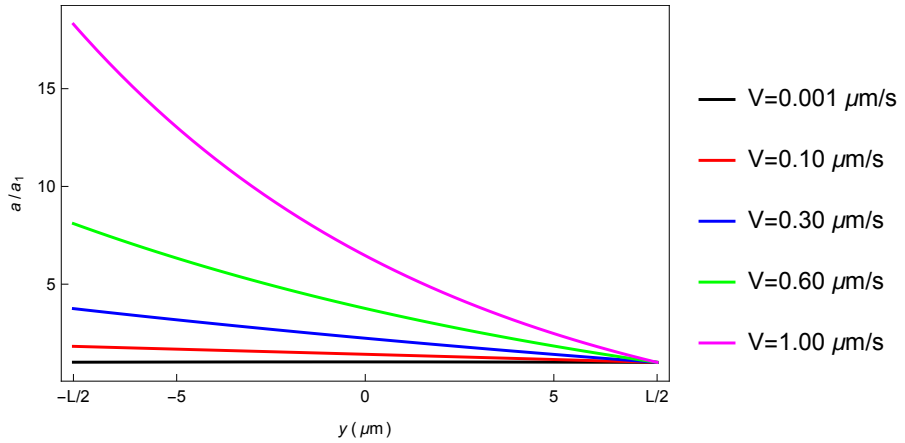

Figure 7: Migrating cell: spatial distribution of monomeric actin for a cell moving in the positive x direction with different (given) migration velocities. Actin distributions are normalized using the value at the leading edge: $a(L/2) = a_1 = 5 \cdot 10^6$, $a(-L/2) = a_2$. We set $a_2 = 1.0078\, a_1$ (black line), $a_2 = 1.82\, a_1$ (red line), $a_2 = 3.75\, a_1$ (blue line), $a_2 = 8.1\, a_1$ (green line), $a_2 = 18.3\, a_1$ (magenta line). Moreover $a_0/\kappa\mu = 0.36$. The remaining model parameters take the values listed in table 1.

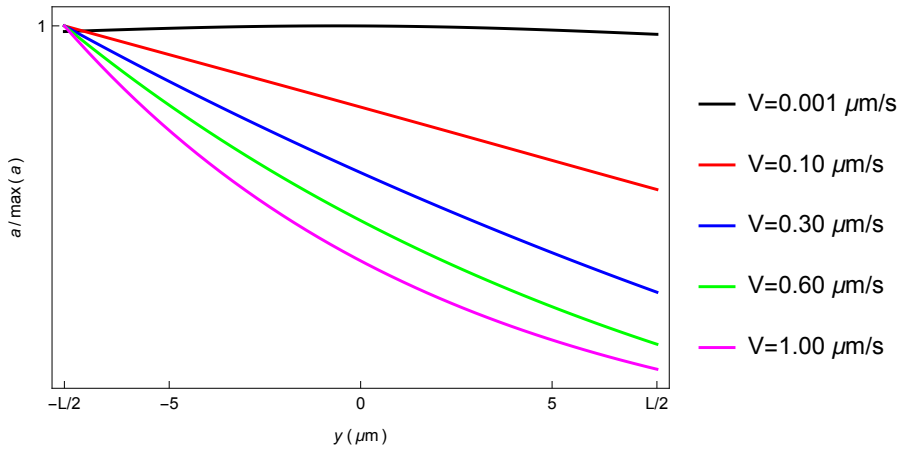

Figure 8: Migrating cell: spatial distribution of monomeric actin for a cell moving in the positive x direction with different migration velocities. Actin distributions are normalized by their maximal absolute values. In each computation $a(L/2) = a_1$, $a(-L/2) = a_2$ with $a_1 = 5 \cdot 10^6$. We set $a_2 = 1.0078\, a_1$ (black line), $a_2 = 1.82\, a_1$ (red line), $a_2 = 3.75\, a_1$ (blue line), $a_2 = 8.1\, a_1$ (green line), $a_2 = 18.3\, a_1$ (magenta line). Moreover $a_0/\kappa\mu = 0.36$. The remaining model parameters take the values listed in table 1.

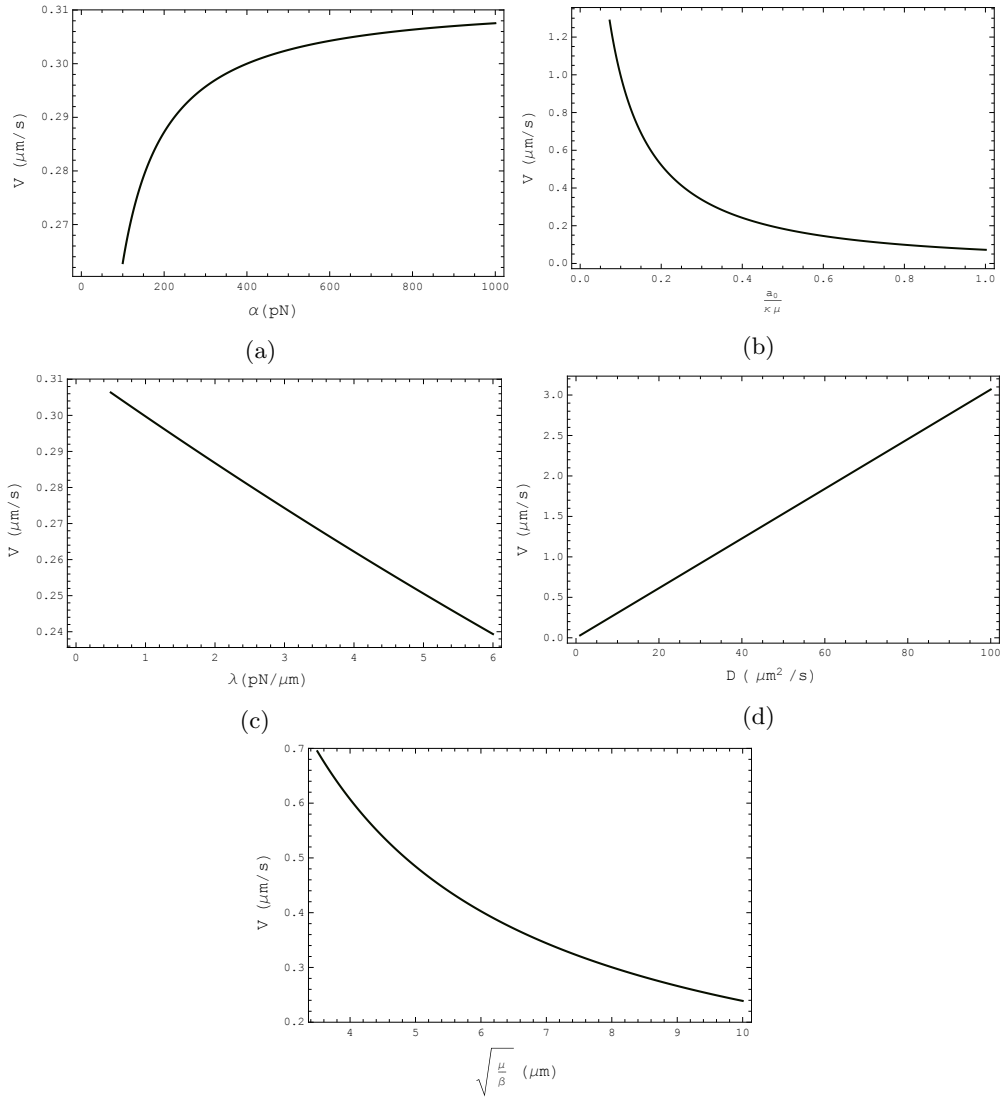

Figure 9: Cell velocity as a function of: (a) α, (b) $\frac{a_0}{\kappa\,\mu}$, (c) λ, (d) D, (e) $\sqrt{\frac{\mu}{\beta}}$. In each computation the fixed parameters take the values given in table 1. Moreover, we set $a(\frac{L}{2}) = a_1 = 5 \cdot 10^6$, $a(-\frac{L}{2}) = a_2 = 4a_1$ and in (a), (b), (c), (d) $\frac{a_0}{\kappa\mu} = 0.33$.

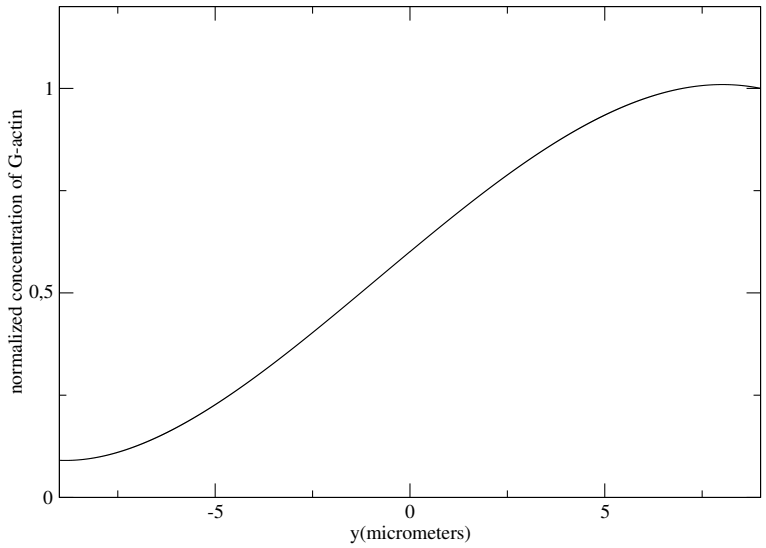

Figure 10: Migrating cell: spatial distribution of polymeric actin for a cell moving in the positive x direction according to (36). Actin distributions is normalized by its maximal value. All the parameters are as listed in table 1.

List of Tables

1 Model parameters taken from the literature on fish keratocytes. 31

Parameter	Physical Meaning	Value	Source
α	contractile active stress	$10^3\,\mathrm{pN}$	[14]
β	friction coefficient	$10^4\,(\mathrm{pN\,s})/\mu\mathrm{m}^2$	[14]
μ	viscosity coefficient	$5 \cdot 10^5\,\mathrm{pN\,s}$	[5]
λ	membrane elastic modulus	$\lambda = 0.5\,\mathrm{pN}/\mu\mathrm{m}$	[4]
D	diffusion coefficient	$10\,\mu\mathrm{m}^2/\mathrm{s}$	[16]

Table 1: Model parameters taken from the literature on fish keratocytes.

MOX Technical Reports, last issues

Dipartimento di Matematica
Politecnico di Milano, Via Bonardi 9 - 20133 Milano (Italy)

19/2016 Guerciotti, B.; Vergara, C.
Computational comparison between Newtonian and non-Newtonian blood rheologies in stenotic vessels

20/2016 Wilhelm, M.; Sangalli, L.M.
Generalized Spatial Regression with Differential Regularization

Guerciotti, B.; Vergara, C.
Computational comparison between Newtonian and non-Newtonian blood rheologies in stenotic vessels

18/2016 Ferroni, A.; Antonietti, P.F.; Mazzieri, I.; Quarteroni, A.
Dispersion-dissipation analysis of 3D continuous and discontinuous spectral element methods for the elastodynamics equation

17/2016 Penati, M.; Miglio, E.
A new mixed method for the Stokes equations based on stress-velocity-vorticity formulation

16/2016 Agosti, A.; Antonietti, P.F.; Ciarletta, P.; Grasselli, M.; Verani, M.
A Cahn-Hilliard type equation with degenerate mobility and single-well potential. Part I: convergence analysis of a continuous Galerkin finite element discretization.

15/2016 Ieva, F.; Paganoni, A.M.
A taxonomy of outlier detection methods for robust classification in multivariate functional data

14/2016 Bonomi, D.; Manzoni, A.; Quarteroni, A.
A matrix discrete empirical interpolation method for the efficient model reduction of parametrized nonlinear PDEs: application to nonlinear elasticity problems

13/2016 Guerciotti, B; Vergara, C; Ippolito, S; Quarteroni, A; Antona, C; Scrofani, R.
Computational study of the risk of restenosis in coronary bypasses

12/2016 Bartezzaghi, A.; Dedè, L.; Quarteroni, A.
Isogeometric Analysis of Geometric Partial Differential Equations